Preprint Title	Synthesis, optical, electronic and solid-state properties of carbonyl-functionalised diketopyrrolopyrroles
Authors	Joshua Humphreys, Ferdinando Malagreca, Paul A. Hume, Flavia Pop, E. Stephen Davies, Stephen P. Argent, Graham N. Newton and David B. Amabilino
Publication Date	04 Sept. 2026
Article Type	Full Research Paper
Supporting Information File 1	Carbonyl DPP ESI.pdf; 5.1 MB
ORCID® iDs	Joshua Humphreys - https://orcid.org/0000-0002-4867-2936; Ferdinando Malagreca - https://orcid.org/0000-0002-2155-1659; Flavia Pop - https://orcid.org/0000-0003-3524-9781; Stephen P. Argent - https://orcid.org/0000-0002-3461-9675; Graham N. Newton - https://orcid.org/0000-0003-2246-4466; David B. Amabilino - https://orcid.org/0000-0003-1674-8462

Synthesis, optical, electronic and solid-state properties of carbonyl-functionalised diketopyrrolopyrroles

Joshua Humphreys,[a, ‡] Ferdinando Malagreca,[a ‡] Paul A. Hume,[b] Flavia Pop,[a §] E. Stephen Davies,[c] Stephen P. Argent,[c] Graham N. Newton[a] and David B. Amabilino[d*]

a GSK Carbon Neutral Laboratories for Sustainable Chemistry, School of Chemistry, University of Nottingham, Triumph Road, Nottingham, NG7 2TU, UK.

b MacDiarmid Institute for Advanced Materials and Nanotechnology and School of Chemical and Physical Sciences, Victoria University of Wellington, Wellington 6010, New Zealand.

c School of Chemistry, University of Nottingham, University Park, NG7 2RD, UK

d Institut de Ciència de Materials de Barcelona (ICMAB-CSIC), Consejo Superior de Investigaciones Científicas, Carrer dels Til.lers, 08193 Cerdanyola del Vallès, Spain

§ Current Address MOLTECH-Anjou, UMR 6200, CNRS, Univ. Angers, 2 bd Lavoisier, 49045 Angers, France

‡ These authors contributed equally to the work presented here.

Abstract

The synthesis, structural and optoelectronic properties of a series of electron deficient chromophores based on benzaldehyde- and benzoate-functionalised diketopyrrolopyrroles (DPPs) is described. All compounds have high molar absorption coefficients and fluorescence quantum yields. The benzoate derivative, with a protonated lactam nitrogen that can engage in hydrogen bonding, shows unusually high solubility in THF. *N*-Alkylation of the lactam unit disrupts the hydrogen bonding of the chromophores, rendering derivatives soluble in solvents ranging in polarity from toluene to acetonitrile, in which they display negative solvatochromism. In the solid state, single crystal structures show that for the benzoate family, *N*-alkylation modulates the π-π stacking interactions from a sandwich interaction between phenyl and lactam moieties to CH-π interactions between adjacent phenyl rings distorted from ideal orthogonality between lactam and phenyl units**.** In contrast, the benzaldehyde derivative displays a similar sandwich interaction to the ester with the unsubstituted lactam. Theoretical mobility measurements based on the crystal packing indicate values approaching 0.05 $cm^2 V^{-1}s^{-1}$ for holes and 0.08 $cm^2 V^{-1}s^{-1}$ for electrons, suggesting promise as potential semiconductors for organic electronic applications. All compounds display multiple redox processes, with each having a single irreversible oxidation process and multiple accessible reversible reduction processes, showing their electron accepting ability. Electron paramagnetic resonance spectroscopy of the singly reduced species shows the delocalisation of the unpaired electron over the whole aromatic part of the molecule. Spectroelectrochemical visible absorption spectra tracking the first and second reduction processes give orders of magnitude increase in their molar absorption coefficient in most cases, attributed to the diradical taking the quinoidal form and suggest suitability for electrochromic applications.

Introduction

Diketopyrrolopyrrole (DPP) derivatives are widely investigated organic semiconductor molecular materials.[1–5] The compound's impressive optical properties, coupled with robust intermolecular interactions between neighbouring chromophores, prompted a surge in research of this family of compounds. Since their discovery,[6] much of the research has focused on synthetic modification to modulate solubility, absorption/emission range, frontier orbital energies, charge carrier mobility and crystal packing, to produce materials with distinct functionality for applications in areas such as organic electronics, biological imaging and sensing. [7-17]

Clearly, the nature of the aryl unit (Ar) of **ArDPP** based structures has a large influence on these properties and crystal structure analysis has also shown that the nature of the alkyl chain – usually used to impart solubility in common organic solvents for processability – can have a significant effect on crystal packing and in turn solid state optoelectronic behaviour.[18-26] For phenyl DPP (**PhDPP)** systems, *N*-alkylation of the lactam unit to negates its hydrogen bonding network that is often present in the pigment species: It significantly alters the intermolecular interactions and degree of planarity of the molecules, and, through this twisting, influences the band gap, reversibility of redox process, stabilisation of radical species and charge transport. On the other hand, the widely-researched thiophene counterparts (**ThDPP**) conserve inter-ring planarity depending on the alkyl unit.[23,27]

In general, in a potential window between +2 and -2 eV with cyclic voltammetry, most reported examples of **PhDPP**s possesses a single reduction process of the DPP acceptor core and multiple oxidation processes related to the aryl unit. Considering DPP as archetypically a D-A-D type structure, with electron rich aryl units flanking the electron deficient core, has resulted in greater investigation of the electrochemical properties of the oxidised species as radical cation and dication species.[24,28-32] Few studies to probe the reduction processes using spectroelectrochemical methods show somewhat similar behaviour for the radical anion species **PhDPP-**type structures,[28] with much grerater absorbance for the reduced species compared to the neutral one, extending to the near IR, with delocalisation of the radical across the whole molecule. The large increase in absorbance for the singly reduced species is not observed for **ThDPP**.[28-29,33,34]

Amongst our own work on the supramolecular and optoelectronic behaviour of DPP-based systems,[35-36] we observed that peripheral functionalisation of **PhDPP** ***NH*** and **PyrDPP** ***NH*** (Pyr = pyridinium) can lead to appreciable improvement in solubility in organic solvents, whilst retaining the favourable planarity and hydrogen bonding network, a key contributor to efficient charge transport.[37] The targeting of highly electron deficient based DPPs (Fig. 1), through increasing the electron deficiency of the aryl unit to 4-pyridinium, resulted in soluble derivatives with the lactam unit free to hydrogen bond, showing the characteristic paraquat-like reversible reduction processes from the pyridinium moiety, in addition to that of the DPP core. This system exhibits

remarkable spectroelectrochemical behaviour, with orders of magnitude increases in molar absorption coefficients (ε) upon reduction (>10 fold increase for the singly and doubly reduced).[36] These polaron- and bipolaron-like absorbance bandss display large colour switching, reminiscent of doped organic conjugated polymers.[38] A quinoidal structure is adopted in the reduced form, the change in band gap manifested in a red shift in absorbance towards the near IR. Reduction of electron deficient quinoidal bithiophenes[39] and electron deficient diene type DPPs[40] leads to an increased absorbance relative to the neutral state for both radical anion and dianion species, but not to the same extent as observed in the pyridinium DPP. The coplanarity of pyridinium and DPP core ring systems in the electron deficient **PyrDPPs** with free NH group is believed to be a major contributing effect to this phenomenon. The remarkable spectroelectrochemical properties suggest promise for electrochromic and molecular logic applications, although reversible processes can be complicated by the change in charge of the molecules. Further work has shown that a phenyl derivative with free NH lactam had appreciable solubility in organic solvents with remarkable supramolecular assembly.[35] The electron rich ether linkage between phenyl ring and substituent group meant that, the compound possesses a single two-electron oxidation process and a single quasi reversible reduction, which renders full spectroelectrochemical exploration unfeasible.

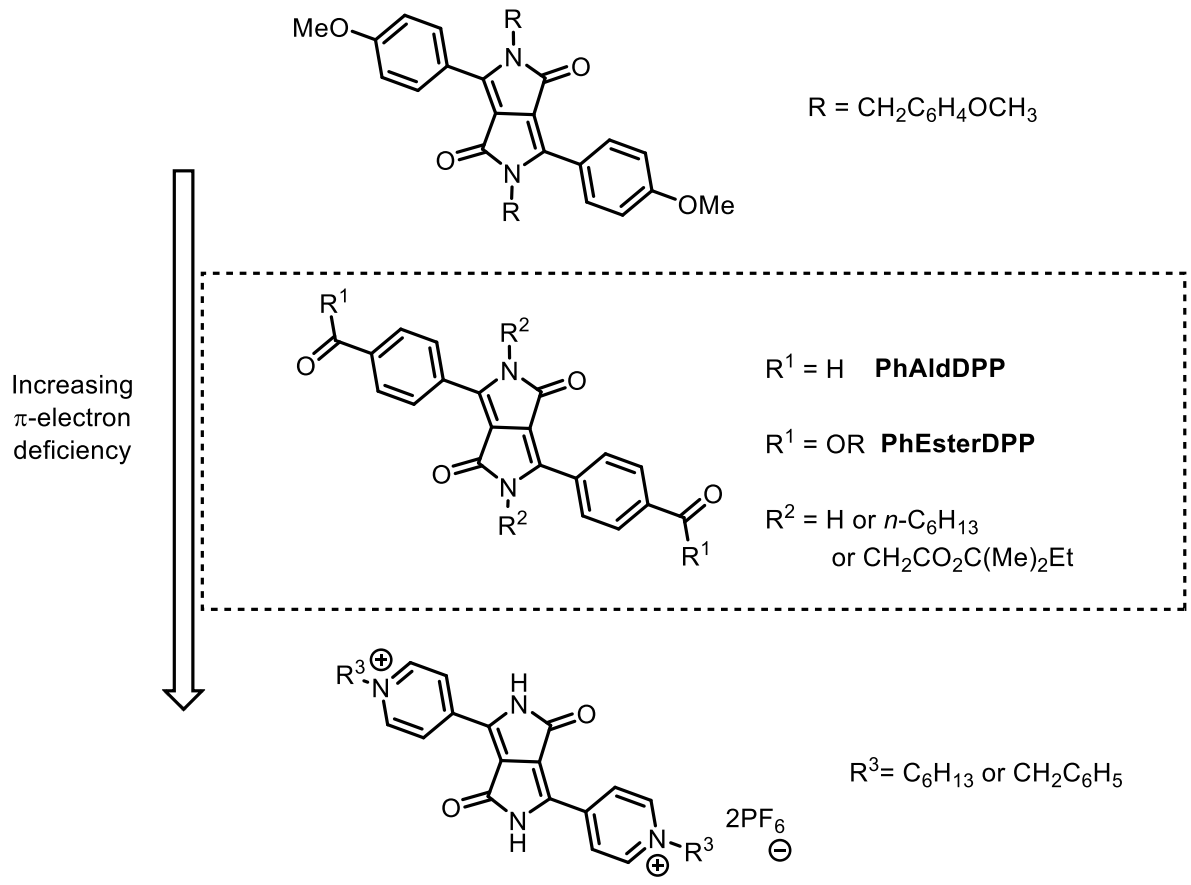

Fig. 1. *DPP systems with increasing π -electron deficiency that have been studied spectroelectrochemically, with the subjects of this study in the dashed box.*

Based on these former works, we looked to synthetically target neutral electron deficient **PhDPP NH** -type systems, where the planar structure is conserved to see if the spectroelectrochemical behaviour and access to quinoidal structure observed in the pyridinium unit is mirrored in other electron deficient DPP molecules, the ultimate aim being to prepare a set of high absorption materials for switchable electrochromic systems.

Benzaldehyde and benzoate ester-decorated DPPs **PhEsterDPP** and **PhAldDPP** (Fig. 1) were identified as viable target systems, given their previous promise as organic solar cell materials,[41,42] capability to further functionalise the systems through conventional or dynamic covalent bonds and ability to coordinate to create larger networked systems as well as the previous success with the ester moiety in creating soluble lactam free **PhDPP**s.[35] The *N*-alkyl variants are also targeted for a direct comparison of electrochemical properties with their **PhDPP NH** parent system, which was not possible previously for **PhOMeDPP NH**,[23,28] owing to solubility constraints of the pigment preventing efficient study of redox chemistry in solution. For those **PhDPP NH** systems that have been studied by CV in the solid state, it has been shown that difficulties arise because of the quality of films deposited on the electrode and dispersion in electrolyte solution, limiting the study of reversible processes.[43] The present work aims to show the influence of functionalisation and intermolecular interactions on the electrochemical stability and optoelectronic behaviour of **PhDPP** based systems through characterising the optical, electronic and solid-state properties to assess the viability of the materials for potential applications and develop structure property relationships for future molecular design.

Results and discussion

Synthetic procedure

To prepare the benzoate-decorated DPP (**PhEsterDPP**), methyl 4-cyanobenzoate was chosen as the starting aryl carbonitrile, using the succinate condensation method for DPP formation. It became apparent that at the elevated temperatures of the reaction, transesterification of the methyl ester to the *t*-amyl derivative arose and by increasing the time of the reaction, full conversion to the *t*-amyl ester (**PhEsterDPP NH**) occurred. The yield of the reaction was improved by replacing diethyl succinate with di-*tert*-amyl succinate (Scheme 1), suppressing the undesirable cyclisation of the succinate via Claisen condensation under basic conditions.[2] The isolated **PhEsterDPP NH** showed remarkably high solubility in THF, uncommon for **DPP NH** species, along with more usual solubility in DMF and DMSO. For comparative purposes, alkylation of the lactam core was performed to negate hydrogen bonding. Employing caesium carbonate as base in acetonitrile,[44] *n*-hexyl and *t*-butyl acetate were chosen as the alkylating units (Scheme 1) and yielded **PhEsterDPP N-Hex** and **PhEsterDPP N-TBA** respectively in moderate yield (21% and 59%), with the compounds displaying high solubility in solvents of varying polarity from toluene to acetonitrile.

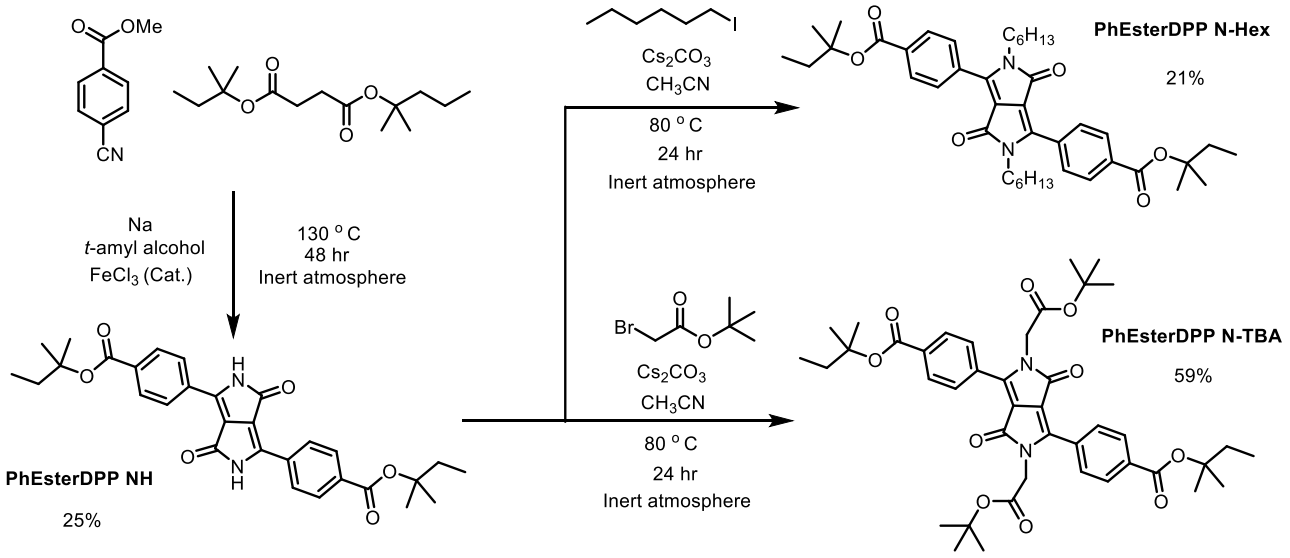

Scheme 1. *Synthetic route and reaction conditions for the formation of* ***PhEsterDPP N-R*** *derivatives (****PhEsterDPP NH, PhEsterDPP N-Hex*** *and* ***PhEsterDPP N-TBA)***

Regarding preparation of benzaldehyde decorated DPPs (**PhAldDPP**), **PhAldDPP N-R** species have previously been isolated through the condensation of the acetal protected carbonitrile *via* the succinate method to form **PhAcetDPP NH** (using a method described previously[45]) followed by *N*-alkylation to **PhAcetDPP NR** and subsequent acid hydrolysis (Scheme 2) to form **PhAldDPP NR**, in a way similar to that described previously.[46] Inspired by this route, attempts were made to transform the isolated **PhAcetDPP NH** to **PhAldDPP NH**, but the insolubility of the materials hindered isolation and subsequent characterisation, thus it was unviable for us to study **PhAldDPP NH** further. For comparison with **PhEsterDPP N-Hex** and **PhEsterDPP N-TBA, PhAldDPP N-EA** was synthesised according to a modified previous procedure (Scheme 2),[44-47] showing good solubility in various solvents.

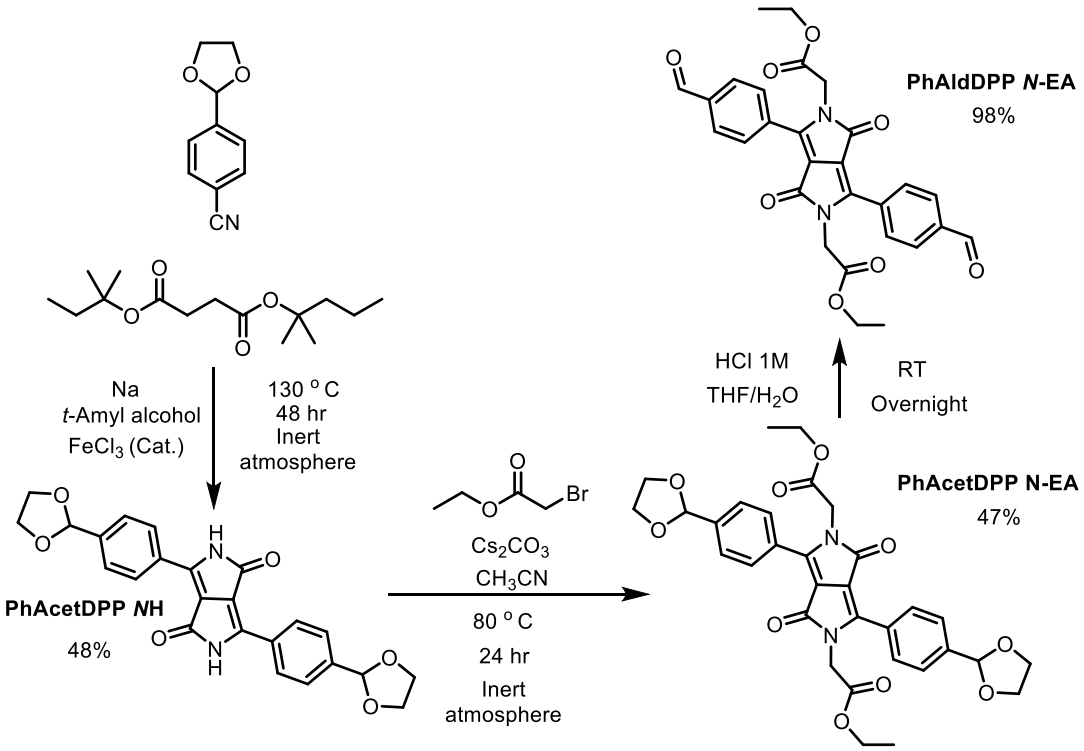

Scheme 2. *Synthetic route and reaction conditions for the formation of* ***PhAldDPP N-EA***

Optoelectronic properties

UV-Visible absorption studies to assess the effect of functionalisation on the optical properties were carried out in THF initially, owing to the high solubility of **PhEsterDPP NH** in the medium. All systems showed typical visible absorption behaviour for **PhDPPs** (Fig. 2),[18-22] with *N*-alkylation leading to a broadening of the main absorption band with overlap of the vibronic structure, coupled with a hypochromic and hypsochromic shift relative to the parent (NH species) arising from the increased dihedral angle between the phenyl and lactam units caused by steric interactions between the hydrogen atoms at the 2-position of the aryl ring with the *N*-alkyl chains. Similar ε values to literature values were observed (Table 1).[18-19,48] The **PhEsterDPP NH** absorption band is bathochromically shifted by 24 nm relative to **PHDPP NH**, an effect attributed to the extended conjugation and electron withdrawing nature of the benzoate group. Additionally, for **PhEsterDPP N-TBA** the electron withdrawing nature of the chain results in a blue shifted absorption band relative to **PhEsterDPP N-Hex.** For **PhEsterDPP N-Hex, PhEsterDPP N-TBA** and **PhAldDPP N-EA** the visible absorption spectra were recorded in a multitude of solvents of varying polarity with all displaying negative solvatochromism (ESI 1.1-1.7).[47]

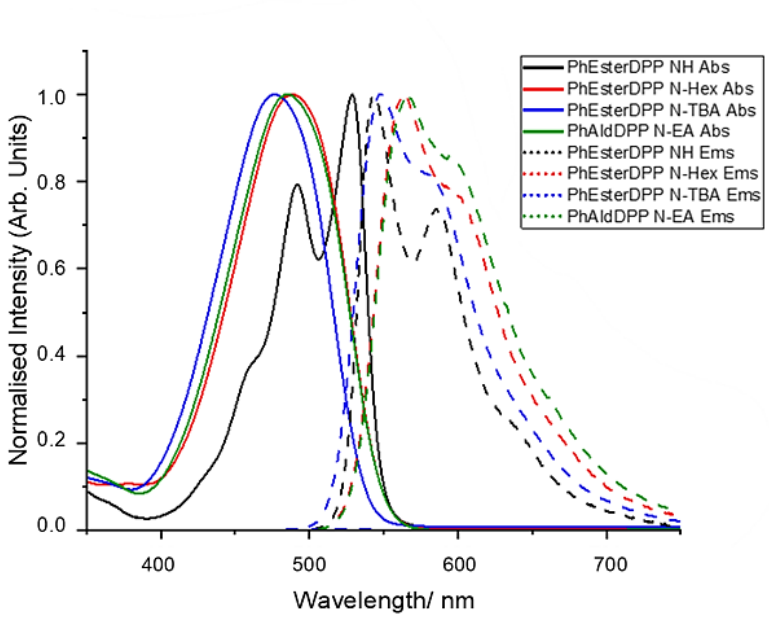

Fig. 2 *UV/Visible absorption and emission spectrum of* ***PhEsterDPP NH, PhEsterDPP N-Hex, PhAldDPP N-EAc*** *and* ***PhEsterDPP N-TBA*** *in THF. Excitation wavelength 470 nm using fluorescein in 0.1M NaOH as reference.*

Table 1. *Photophysical properties and experimental frontier orbital energy levels of* ***PhEsterDPP NH, PhEsterDPP N-Hex, PhAldDPP N-EAc*** *and* ***PhEsterDPP N-TBA***

Compound	Absorption λ_{max} [nm]	Emission λ_{max} [nm]	ε [dm^3mol^{-1} cm^{-1}]	Stokes shift [nm]	Φ	HOMO [eV]	LUMO [eV]	Electronic Eg [eV]
PhAldDPP *N*-EA	486	565 [a]	16,200	79	0.79[b]	-5.73[d]	-3.60 [d]	2.13 [d]
PhEsterDPP *N*H	529	544[a]	29,400	14	0.85[c]	-5.43 [d]	-3.60 [d]	1.83 [d]
PhEsterDPP *N*-Hex	488	563 [a]	23,200	75	0.84[c]	-5.54 [d]	-3.56 [d]	1.98 [d]
PhEsterDPP *N*-TBA	477	548[a]	19,400	71	0.80[b]	-5.65 [d]	-3.60 [d]	2.05 [d]

[a] *Excitation wavelength 470 nm.* [b] *Quantum yield calculated by Integrated Sphere.* [c] *Quantum yields were calculated by comparison with the fluorescence observed for fluorescein (F = 91 in NaOH) under identical conditions of irradiation.* [d] *Experimental value determined from cyclic voltammetry measurements in DMF (***PhEsterDPP *N*R***) or acetonitrile (***PhAldDPP N-EA****) solution containing 1mmol compound and [n-Bu_4N][PF_6] (0.2M). Potentials are referenced against the Fc/Fc^+ couple employed as an internal standard.*

In terms of fluorescence, typical emissive behaviour is observed for **PhDPP** analogues regarding band shape and quantum yield (Table 1).[21-23,48-49] **PhEsterDPP NH** possesses mirror image absorption and emission profiles and a small Stokes shift (14 nm), with retention of vibronic structure (Fig. 2), whereas upon *N*-alkylation, (**PhEsterDPP N-Hex** and **PhEsterDPP N-TBA)** there is loss of molecular planarity and symmetry, leading to non-mirror image absorption and emission profiles, a large Stokes shift (≈70 nm) (Fig 2 and ESI 1.8-1.11) and an increase in vibronic structure in emission, suggesting planarization of the molecule in the excited state.[28] For **PhEsterDPP N-TBA**, the bathochromic shift in emission profile relative to **PhEsterDPP NH** is much more moderate**,** however the Stokes shifts are of similar magnitude, suggesting the electronic nature of the side chain is likely responsible. The emission profile of **PhAldDPP N-EA** is again typical of *N*-alkylated **PhDPP NR** systems.

In terms of absorption in the solid state (ESI 1.13-1.20), **PhEsterDPP NH** shows a bathochromic shift of the spectrum relative to solution, indicative of *J*-type aggregation, attributed to hydrogen bonding and π-π stacking intermolecular interactions in the solid state and a visible broadening of the film.[46] **PhEsterDPP N-Hex** also shows a bathochromic shift of the absorption maxima, although less moderate. Regarding emission, for **PhEsterDPP NH** strong intermolecular hydrogen bonding and π stacking interactions quench emission in the solid state. For **PhEsterDPP N-Hex**, *N*-alkylation does not allow the hydrogen bonded network and modulates stacking resulting

in a broader emission compared with solution, with a loss of vibronic structure and a larger Stokes shift (ESI 1.17-1.20). **PhAldDPP N-TBA** has previously shown interesting solid-state absorption/emission behaviour.[45]

Cyclic Voltammetry studies

Cyclic voltammetry measurements (Fig. 3 and ESI 1.21-1.44) indicate all four derivatives possess one irreversible oxidation process, modulated slightly by the presence of the alkyl chain for the **PhEsterDPP N-R** family. Regarding reduction, **PhAldDPP N-EA** displays three quasi reversible reduction peaks at -1.23, -1.54 and -2.42 V, whereas all the **PhEsterDPP NR** family show two reversible reduction processes with a negligible difference in potential (ESI 1.26-1.44). As expected, *N* alkylation widens the band gap (≈ 2.0 eV) as the aryl rings twist out of the plane of the DPP core, lowering effective conjugation compared with the parent **PhEsterDPP NH**,(Table 1 and ESI 1.12), that has a smaller band gap than observed for other **PhDPP NH** species.[43] The precursor **PhAcetDPP N-EA** possesses a single quasi-reversible oxidation and two one electron reductions, the first quasi-reversible and second irreversible (ESI 1.21-1.25).

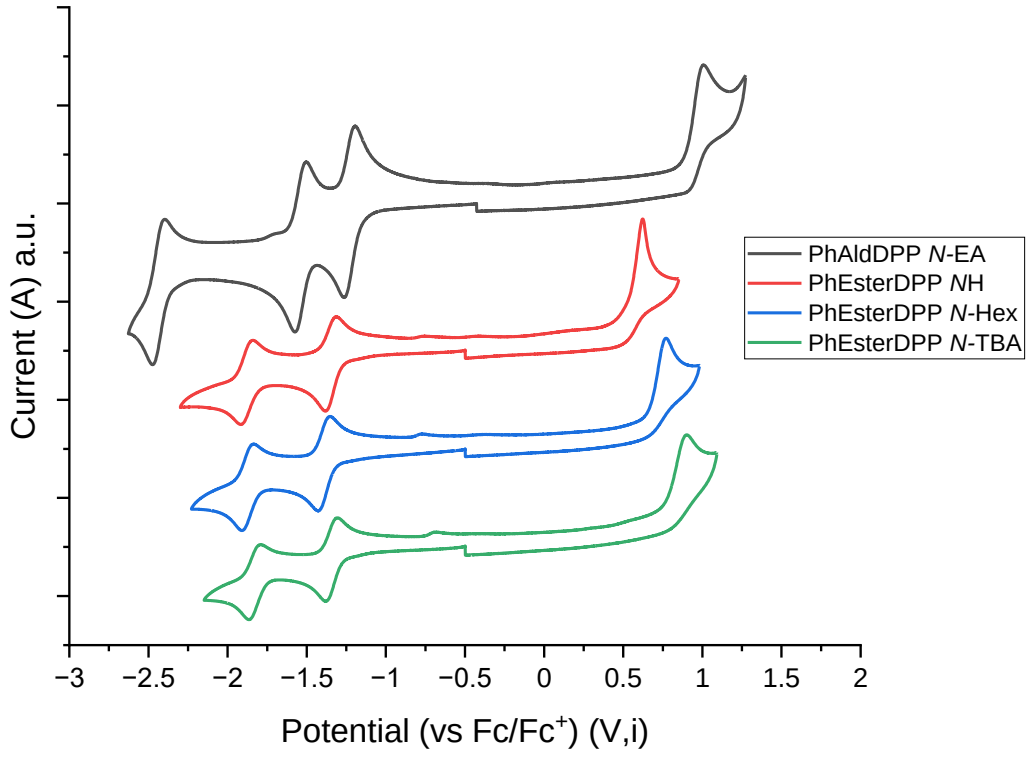

Fig. 3. *Cyclic voltammograms were obtained in DMF* ***(PhEsterDPP NR)*** *or acetonitrile* ***(PhAldDPP N-EA)*** *solution containing [n-Bu$_4$N][PF$_6$] (0.2M) supporting electrolyte at a scan rate of 100 mVs^{-1}, under an argon atmosphere, with a glassy carbon working electrode, a Pt wire secondary electrode and a saturated calomel reference electrode. Potentials are plotted against the Fc$^+$/Fc couple employed as an internal standard*

Spectroelectrochemical properties.

To evaluate potential application as electrochromic materials, UV-vis-NIR spectroelectrochemical studies were undertaken on the reduction processes of these molecules. The absorption spectra of the singly- and doubly-reduced forms of **PhEsterDPP NH,** *and* **PhAldDPP N-EA** are shown in Figs. 4 and 5 (**PhEsterDPP N-TBA,** and **PhEsterDPP N-Hex** *(*ESI 1.45 -1.46). In all cases, the clean formation of the new radical anion species from the neutral system are evidenced by the presence of an isosbestic point, indicating direct conversion without formation of a long lived intermediate (ESI 1.47).

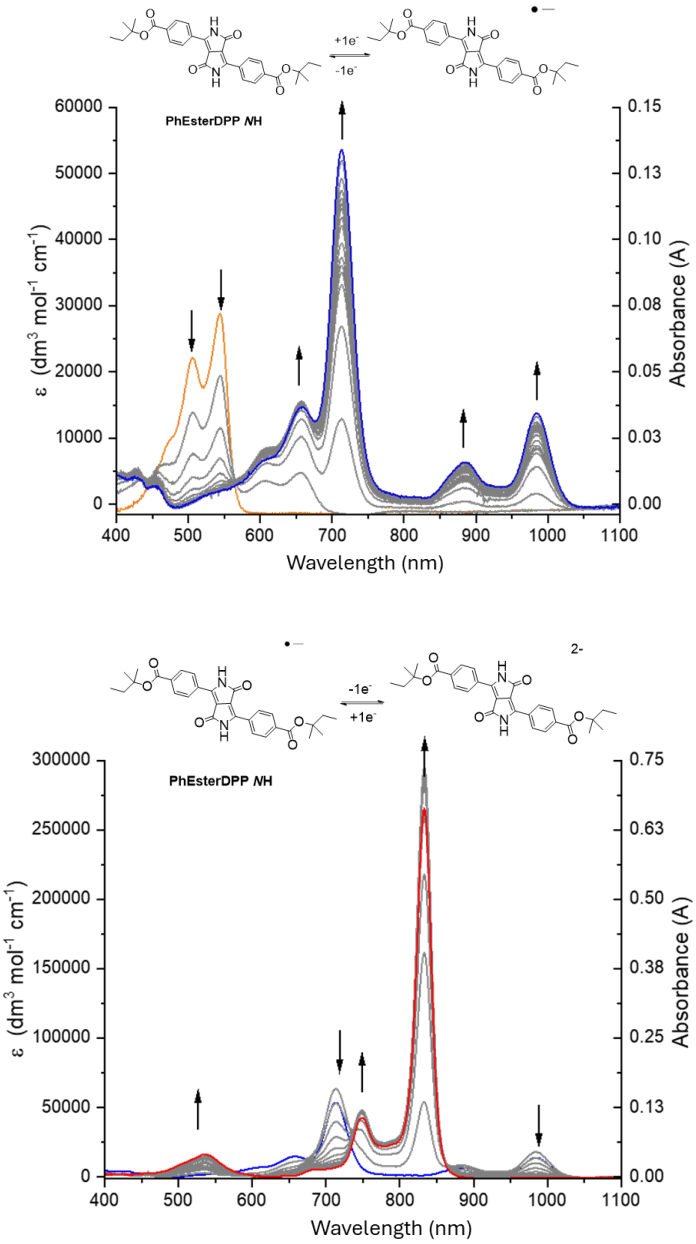

Fig. 4. *UV-visible absorption monitoring of the first reduction process (top) and second reduction process (bottom) of* ***PhEsterDPP NH.*** *In each graph the orange line represents the neutral species, the blue line represents the*

first reduced species and the red line represents the second reduced species. Spectra were recorded in DMF containing [n-Bu_4N][PF_6] (0.2M) as the supporting electrolyte at 273K.

To reach the second reduced state, each goes *via* the singly reduced state indicating thermodynamic stability of the anion radical under the conditions of the experiment. For **PhEsterDPP NH,** the spectra were collected at two different concentrations, owing to the enormous increase in ε value for the doubly reduced species saturating the detector (Fig. 4 and ESI 1.48). For the single electron reduction, the main bands in the visible region at 532 nm (29,000 dm^3mol^{-1} cm^{-1}) and 495 nm (22,000 dm^3mol^{-1} cm^{-1}) diminish and new bands appear towards the NIR at 657 nm (14,000 dm^3mol^{-1} cm^{-1}), 714 nm (53,000 dm^3mol^{-1} cm^{-1}), 886 nm (6,000 dm^3mol^{-1} cm^{-1}), and 984 nm (14,000 dm^3mol^{-1} cm^{-1}). For the two-electron reduction**,** the absorption bands of the mono-reduced **PhEsterDPP NH** disappear and three new bands are observed at 538 nm (16,000 dm^3mol^{-1} cm^{-1}), 748 nm (46,000 dm^3mol^{-1} cm^{-1}) and 833 nm (296,000 dm^3mol^{-1} cm^{-1}). For **PhAldDPP *N*-EA** (Fig. 5), the single electron reduction results in the loss of bands at 487 nm (17,000 dm^3mol^{-1} cm^{-1}) and 295 nm (44,000 dm^3mol^{-1} cm^{-1}) and emergence of three intense bands, one at 380 nm and two of them at low energy at 732 nm (71,000 dm^3mol^{-1} cm^{-1}) and 1036 nm (29,000 dm^3mol^{-1} cm^{-1}), along with a less intense broad band at 920 nm (9,000 dm^3mol^{-1} cm^{-1}). For the two-electron reduction, the low energy bands are replaced by a new broad band in the visible region 566 nm (12,000 dm^3mol^{-1} cm^{-1}). and a very intense band at 867 nm (137,000 dm^3mol^{-1} cm^{-1}) with a shoulder at 780 nm (42,000 dm^3mol^{-1} cm^{-1}).

For **PhEsterDPP N-Hex** and **PhEsterDPP N-TBA** (ESI 1.45 -1.46)**,** the spectra of the singly reduced species are similar with the band in the visible region at ≈ 490 nm (≈ 20,000 dm^3mol^{-1} cm^{-1}) lost in both, and two new bands appear at ≈ 700 nm (≈ 90 -150,000 dm^3mol^{-1} cm^{-1}) and ≈ 850 nm (≈ 15- 20,000 dm^3mol^{-1} cm^{-1}). In the UV region, the band at ≈290 nm (40-50,000 dm^3mol^{-1} cm^{-1}) diminish and two small new bands are formed at ≈ 360 nm (≈ 15-30,000 dm^3mol^{-1} cm^{-1}). For the 2 electron reduction, initially formed bands similar to **PhEsterDPP NH** at ≈ 520 nm (≈ 45-55,000 dm^3mol^{-1} cm^{-1}) and at ≈820 nm (≈ 50-60,000 dm^3mol^{-1} cm^{-1}) are noted, with an additional band at ≈ 690 nm (≈ 25,000 dm^3mol^{-1} cm^{-1}) observed for **PhEsterDPP N-TBA**. After a certain concentration of second reduced species, the band at 690 nm and 820 nm decreases until it completely disappears for **PhEsterDPP N-Hex**, indicating some instability under the conditions of the experiment.

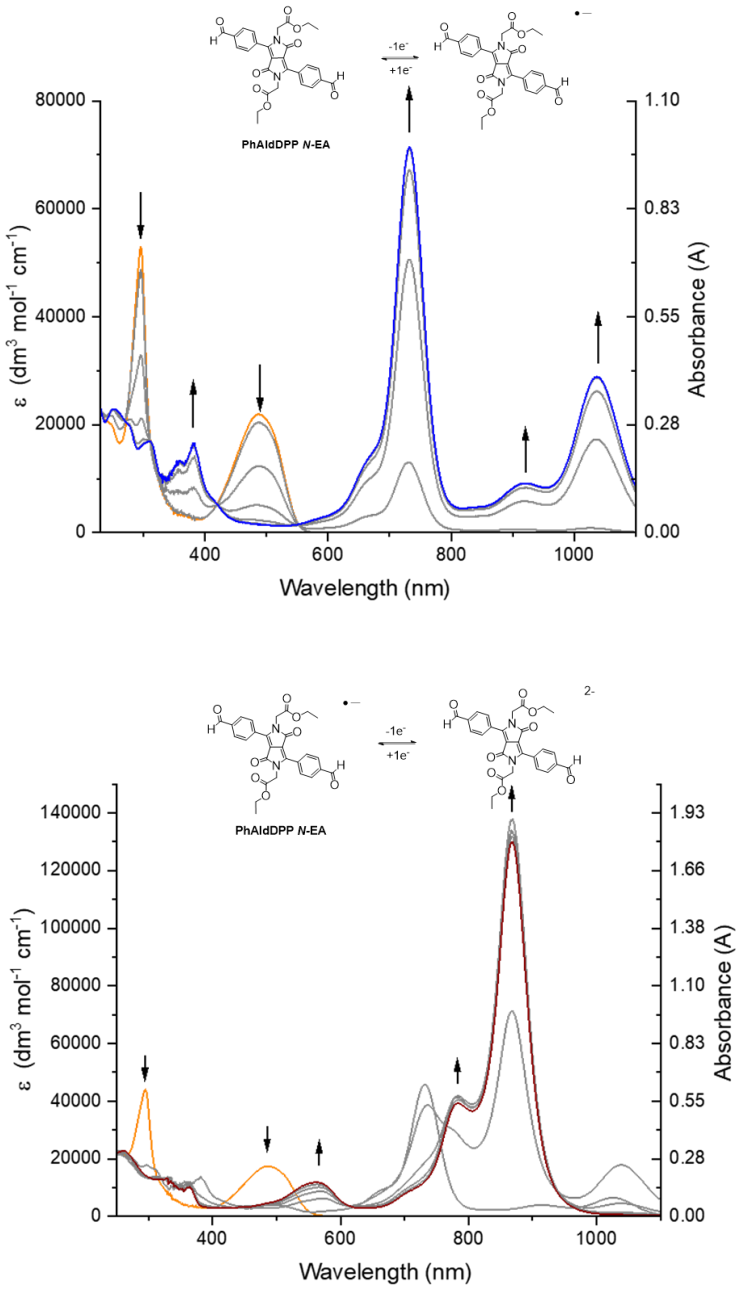

Fig. 5. *UV-visible absorption monitoring of the first reduction process (top) and second reduction process (bottom) of* ***PhAldDPP N-EA.*** *In each figure the orange line represents the neutral species, the blue line represents the first reduced species and the red line represents the second reduced species. Spectra were recorded in acetonitrile containing [n-Bu$_4$N][PF$_6$] (0.2M) as the supporting electrolyte at 273K.*

Regarding stability, re-oxidation of the singly reduced solution for **PhEsterDPP N-H** regenerates the absorption profile of the neutral species, with a marginal loss of absorbance of the main visible band (ESI 1.49-1.50). This situation is also true for re-oxidation of the doubly reduced molecule, indicating limited decomposition over the experimental timescale (2-3 hours) and under those conditions. The redox processes show appreciable stability over spectroelectrochemical

experiments and cycling, suggesting their viability as candidates for electrochromic applications. For the *N*-alkylated compounds (**PhEsterDPP *N*-TBA, PhEsterDPP *N*-Hex** and **PhAldDPP *N*-EA)**, re-oxidation of the singly reduced solution shows a small loss of absorbance of the main visible band (ESI 1.51-1.53), whereas re-oxidation of the doubly reduced compound shows increased intensity loss across all the spectral rage, indicating that the doubly reduced species are susceptible to decomposition over this longer experimental timescale and that alkylation reduces the stability of the DPP compared with the unsubstituted lactam compounds.

For pyridinium derivatives of DPPs containing hexyl and benzyl substituents we have observed previously large increases in **ε** values upon reduction with the first reductions show an increase of 250% and 320%, for hexyl and benzyl, respectively whilst 2nd reductions show increases of 950% and 1600%, respectively.[36] For **PhEsterDPP *N*-H** and **PhAldDPP *N*-EA,** accompanying the shift of the main absorption bands towards the near IR, the **ε** value of the λ_{max} increases by 80% and 320%, respectively for the radical anion and 920% and 700%, respectively for the doubly reduced species relative to the neutral compound (Table 2). For **PhEsterDPP *N*-Hex** and **PhEsterDPP *N*-TBE, the** increases in extinction coefficient values of 355 % and 625 % are observed for the radical anion but unlike the previous compounds, the increase for the doubly reduced is more moderate (120% and 165%) and could be attributed to the instability of these systems observed over the duration of the experiment. For such seemingly similar reversible reduction processes indicated by cyclic voltammetry for the **PhEsterDPP** family and similarity in the radical anion spectral performance, it is the second reduction to the dianion where the differences lie. The planar **PhEsterDPP *N*-H** derivative, shows an intense red shifted absorbance, probably arising from the ability to readily access the quinoidal form for strong intermolecular interactions between chromophores when compared with the twisted structures of the alkyl-substituted compounds.

PhDPP derivatives have shown increases in molar absorption upon reduction previously, but these are more moderate than observed here.[28, 30-32, 50] It has been shown that formation of radical anion for *N*-alkylated **PhDPP** results in planarisation and similar spectra observed for the alkyl systems with regards to increased absorbance for the radical anion.[51] This planarisation is ratified by the larger stokes shift observed previously, which suggests a geometry change in the excited state relative to the ground state.[28] The behaviour and peaks for the *N*-alkylated derivatives are typical of radical anions for **PhDPP** previously observed and can be considered to delocalised across the whole system. The twisted nature breaks the effective conjugation length over which the polaron is likely to delocalise. Those planar systems associated with the quinoidal form show greater delocalisation and stronger absorbance. Typically for **PhDPP** based systems, the radical anion shows consistent behaviour in terms of peak position and increase in absorbance relative to the neutral state (2-3 times increase).

Given the observed results with both carbonyl and pyridinium based DPPs, it can be assumed that this behaviour is characteristic of electron deficient systems, where the electron withdrawing group is present at the 4-position

of the aryl unit, given the fact that substitution at the 3-position for the pyridinium derivatives resulted in similar moderate values as observed for furan and thiophene derivatives.[28] The large increase in **ε** is therefore attributed to the quinoidal form which affords better overlap between ground state and excited state orbitals in the DPP core, which was previously inferred and is favoured and readily accessible where planarity is retained.[36] Given the electron rich nature of DPPs, radical cation and dication species have been explored to a greater extent, especially in electrochromic polymer DPP systems, owing to the increased conjugated backbone and planarity of said systems resulting in reduced molecular structure changes upon polaron formation and delocalisation across longer length scales, helping to increase charge transport.[510-521] The spectroelectrochemical behaviour observed here correlates with that shown by electron deficient DPPs upon doping,[36,39,53] with polaron formation resulting in strong mid UV absorption near IR and bipolaron showing a slightly blue shifted near IR absorbance attributed to change in band gap.

Table 2. *Spectroelectrochemical properties (λ and ε) of 1st and 2nd reduction process of* ***PhEsterDPP NH, PhEsterDPP N-TBA, PhEsterDPP N-Hex*** *and* ***PhAldDPP N-EA*** *compared with neutral starting compounds*

Compound	**Neutral compound λ / nm** (ε/ dm^3mol^{-1} cm^{-1})	**1st reduction λ / nm** (ε/ dm^3mol^{-1} cm^{-1})	**2nd reduction λ / nm** (ε/ dm^3mol^{-1} cm^{-1})
PhAldDPP *N*-EA	486 (17,000), 295 (44,000)	732 (71,000), 920 (9,000) 1036 (29,000)	566 (12,000), 780 (42,000), 867 (137,000)
PhEsterDPP *N*H	532 (29,000), 495 (22,000)	657 (14,000), 714 (53,000), 886 (6,000), 984 (14,000)	538 (16,000), 748 (46,000), 833 (296,000)
PhEsterDPP *N*-Hex	488 (20,000), 288 (39,000)	365 (18,000), 700 (91,000), 854 (14,000)	528 (44,000), 817 (diminishes)
PhEsterDPP *N*-TBA	486(20,000), 285 (51,000)	360 (27,000), 688 (145,000), 847 (20,000),	520 (53,000), 688 (25,000), 815 (50,000)

Spectra were recorded in DMF ***(PhEsterDPP NR)*** *or acetonitrile* ***(PhAldDPP N-EA)*** *containing [n-Bu_4N][PF_6] (0.2M) as the supporting electrolyte at 273K.*

Electron paramagnetic resonance (EPR) studies.

EPR spectroscopy confirmed the formation of radical anions for the singly reduced forms of **PhAldDPP N-EA**, **PhEsterDPP NH**, **PhEsterDPP N-Hex** and **PhEsterDPP N-TBA** (Fig. 6 and ESI 1.54-1.56)**.** For **PhAldDPP N-EtAc**, simulation of the EPR spectra showed two sets of four equivalent protons (Fig. 6, 1.652 x 10^{-4} cm^{-1} and 0.519 x 10^{-4} cm^{-1}) and two equivalent nitrogen atoms (0.982 x 10^{-4} cm^{-1}) indicative that the electron is delocalised across the π- framework of the molecule. This effect is likely the case for the other derivatives (ESI 1.54-1.56) given their extensive hyperfine

coupling, which were unable to be modelled owing to the complexity of the signals. The hyperfine coupling is consistent with the complexity observed in other **PhDPP** based radical anions,[28] enhancing the intermolecular interactions (π-π stacking) between systems in this doped state.

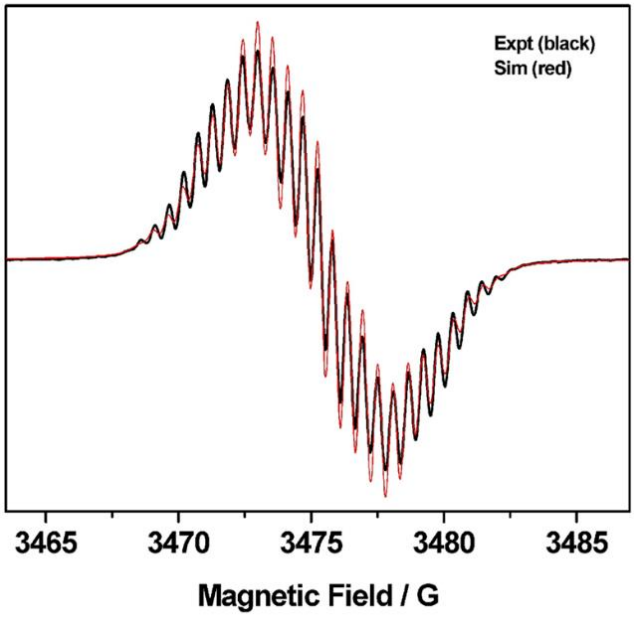

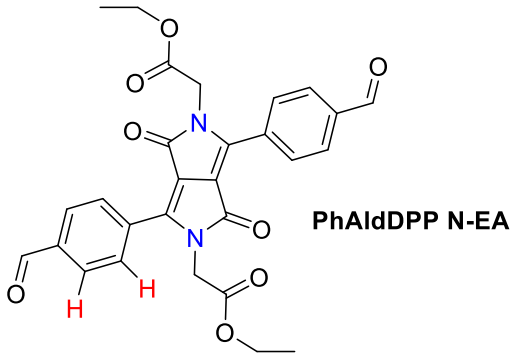

Fig. 6. *Experimental (Black line) and simulated (Red line) EPR spectra of singly reduced **PhAldDPP N-EA** Spectra were recorded in acetonitrile containing [n-Bu$_4$N][PF$_6$] (0.2M) as the supporting electrolyte at 273K. Structure of **PhAldDPP N-EA** with the highlighted atoms (H, N) interacting with the paramagnetic radical.*

Theoretical calculations

Time-dependent density functional theory (TD-DFT) calculations are consistent in terms of oscillator strengths and changes in λ_{max} with the spectroelectrochemical measurements. The neutral forms have predicted absorption maxima at ~500 nm, that are well-described by a single HOMO→LUMO orbital transition.[50] One-electron reduction results in the formation of a weak absorption band at 850-1000 nm, in addition to a stronger absorption peak at ~700 nm. The lower energy band is dominated by SOMO→LUMO (excitation amplitude 0.86), while the band at 700 nm is mainly HOMO→SOMO (excitation amplitude 0.85) in character. The intense absorption of the

doubly reduced compounds around 700-740 nm arises from HOMO→LUMO transitions. These observations are consistent with previous spectroelectrochemical studies of one electron reduction of *N*-alkylated **PhDPP NR** systems,[28] where upon single electron reduction new bands appear at ≈620 nm (HOMO-SOMO) and in the 800 nm region (SOMO-LUMO), with an absorbance increase of ≈180 % and spin density distributed over the entire molecule. Additionally, previously a DFT study of **PhDPP** and **PhDPP NR** computed that the radical anion forms underwent a greater planarization compared with the neutral molecule than the radical cation form.[54]

For the neutral compounds, the bulk electron density distibutions in the ground state is localized on the DPP core in the HOMO,[24,28,50] whereas for the LUMO there is greater delocalization along the long axis by assuming a quinoidal structure. (Figs. 7 and 8 and ESI 1.57-1.59). The large quadrupole moment of the ground state relative to the excited state accounts for the negative solvatochromism previously observed.

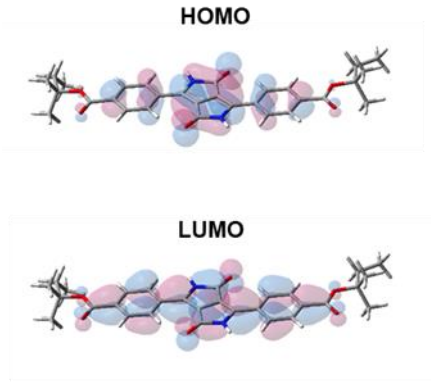

Fig 7. Calculated HOMO and LUMO for **PhEsterDPP NH**

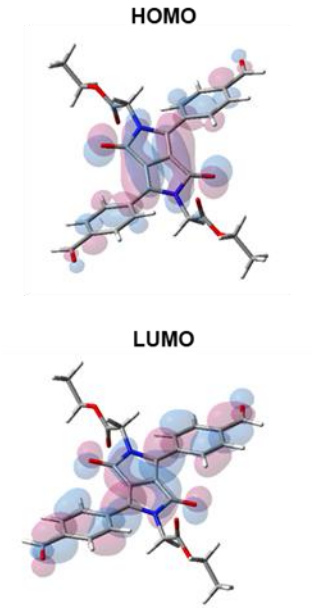

Fig 8. Calculated HOMO and LUMO for **PhAldDPP N-EA**

Single Crystal Structures

Single crystals of **PhAldDPP N-EA**, its precursor **PhAcetDPP N-EA (ESI)** and **PhEsterDPP NH, PhEsterDPP N-TBA** and **PhEsterDPP N-Hex** were obtained through slow evaporation of solvents (ESI 1.60 for details) and the structures were resolved through single crystal X-ray diffraction measurements. **PhEsterDPP NH** has aryl-lactam dihedral angles of 5.70° and 10.7° respectively for the two symmetry independent units (Table 3), reflecting the relative planarity of the system, given its unfunctionalized lactam core.[43,55-58] The *N*-alkylated compounds show larger aryl-lactam dihedral angles of 40.1° and 43.6° for **PhEsterDPP N-Hex** and 35.3° for **PhEsterDPP N-TBA** as the aryl units twist out of the DPP core plane.[59] This effect accounts for the observed blurring of vibronic structure of the absorption band, hypsochromic shift relative to the parent system and increased Stokes shift for these systems.[21-22] In addition, the alkyl chain is twisted out of the plane of the DPP core by 13.5° and 11.1° for **PhEsterDPP N-Hex** and 15.0° for **PhEsterDPP N-TBA** (Table 3). **PhAcetDPP N-EA** (ESI 1.63-1.64) gives similar aryl-lactam (32.7°) and alkyl-lactam dihedral angles (14.0°) to **PhEsterDPP N-TBA**. Upon cleavage of the acetal (**PhAldDPP N-EA)** there is a considerable reduction in the aryl-lactam (20.8° and 21.5°) and alkyl-lactam (7.10° and 7.30°) dihedral angles, which we assign to the reduction in steric bulk, as seen previously in a conceptually related case.[23]

Regarding intermolecular interactions, **PhEsterDPP NH** displays substantial π- π contacts (Fig 9), with sandwich type interactions between phenyl and lactam rings at centroid-centroid distances of 3.62 Å and 3.65 Å respectively, coupled with hydrogen bonds between the NHs and carbonyls on lactams of adjacent molecules at distances of 1.96 Å (ESI 1.65). In contrast, **PhEsterDPP N-Hex** displays CH- π interactions between phenyl rings on neighbouring molecules at a distance of 3.68 Å. (Fig. 9), in addition to a slipped π–π interaction between lactams of 4.82 Å (ESI 1.65). **PhEsterDPP N-TBA** also displays a CH-π interaction but in contrast, this is between phenyl and lactam moieties at an elongated distance of 4.52 Å, with an additional phenyl-phenyl slipped-stacking interaction (5.84 Å) (ESI 1.66). **PhAldDPP N-EA** shows a relatively short interaction between lactam and phenyl moieties, distorted from an ideal sandwich type interaction, at distances of 3.76 Å and 3.78 Å. Additionally, the aldehyde moiety displays hydrogen bonding with the carbonyl of lactam at a distance of 2.523 Å (ESI 1.68). This packing is similar to **PhEsterDPP NH**, with the relative planarity of both systems a possible explanation for the conserving of these interactions, although for **PhAldDPP *N*-EA** the π stacking is distorted and the hydrogen bond interaction elongated, accompanied by the increased aryl dihedral angle. Additional less well defined interactions are also evident in the crystal packing (ESI 1.69-1.73).

In terms of molecular packing, **PhEsterDPP NH** packs in a lamellar 1D structure (ESI 1.74), whereas **PhEsterDPP N-Hex, PhAldDPP N-EA** and **PhAcetDPP N-EA** pack in a more habitual herringbone arrangement observed for other *N*-alkylated **PhDPP** systems (ESI 1.75-1.77),[23,25] In contrast, **PhEsterDPP N-TBA** packs in a lamellar

fashion, likely conserving the packing of its parent at the detriment of closer π contacts (ESI 1.79). All systems display lateral, longitudinal and vertical offsets between neighbouring DPPs, ranging from 0.31-5.75 Å, 2.49-4.88 Å and 2.10-3.32 Å respectively. (ESI 1.79-1.84)

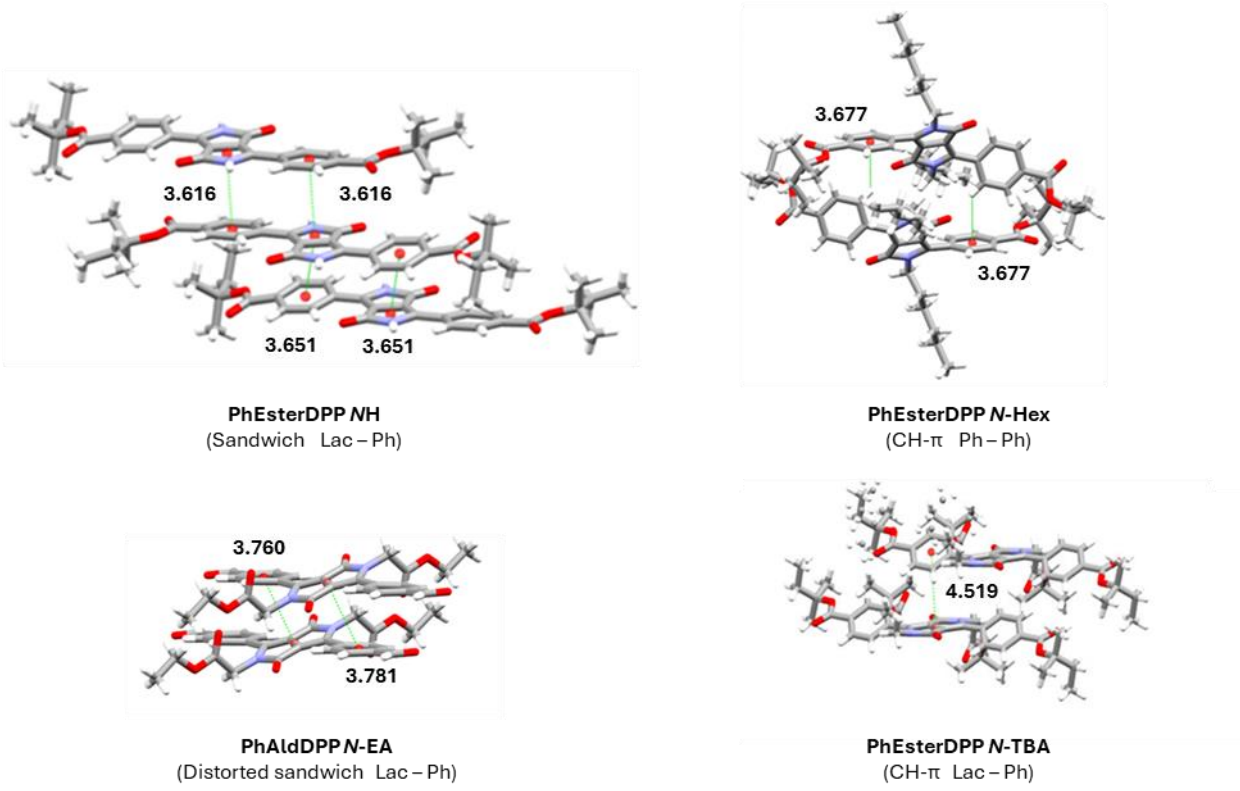

Fig. 9. *Main π system interactions of* ***PhAldDPP N-EA****,* ***PhEsterDPP NH, PhEsterDPP N-TBA and PhEsterDPP N-Hex***

Table 3. *Solid state interactions, packing and calculated hole mobility values for* ***PhAldDPP N-EtAc****,* ***PhEsterDPP NH,*** ***PhEsterDPP N-TBE*** *and* ***PhEsterDPP N-Hex*** *obtained from single crystal structures*

Compound	**DPP aryl-lactam dihedral (°)**	**DPP alkyl-lactam dihedral (°)**	**π -π stacking interaction** centroid to centroid **(Å)**	**H bonding (Å)**	**Bulk packing**	**Calculated mobility ($cm^2 V^{-1}s^{-1}$)**
PhEsterDPP *N*H	5.70, 10.7	n/a	3.62 (Sandwich Lac-Ph)	1.96,	Lamellar 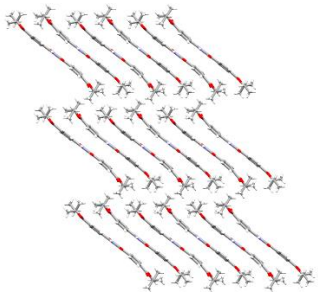	4.70×10^{-2} (Hole) 8.2×10^{-2} (Electron)
PhEsterDPP *N*-Hexyl	40.1, 43.6	13.5, 11.1	3.68 (CH- π Ph-Ph) 4.82 (Lac-Lac slip stack)	n/a	Herringbone 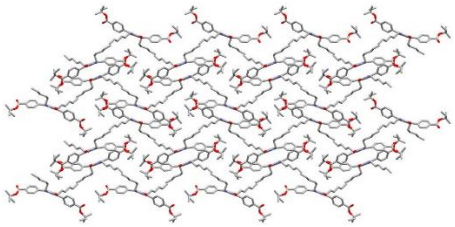	4.00×10^{-3} (Hole) 9.0×10^{-4} (Electron)
PhEsterDPP *N*-TBA	35.3	15.0	4.52 (CH- π Lac-Ph) 5.84 (Ph-Ph slip stack)	n/a	Lamellar 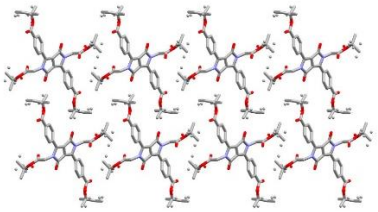	5.30×10^{-4} (Hole) 6.5×10^{-3} (Electron)
PhAldDPP *N*-EA	20.8, 21.5	7.1, 7.3	3.76, 3.78 (Distorted sandwich Lac-Ph)	2.53	Herringbone 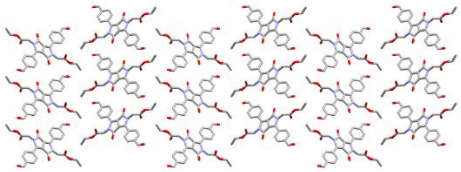	3.25×10^{-2} (Hole) 3.8×10^{-3} (Electron)

The crystal structure of **PhAldDPP N-EA** shows appreciable difference from the literature compound **PhAldDPP N-TBA**.[18] For **PhAldDPP N-TBA** hydrogen bonds are slightly elongated for (2.53 Å) compared with **PhAldDPP N-EA** (1.96 Å) and the aryl-lactam dihedral angle is increased by ≈10° (Table 3). Additionally**,** the alkyl-lactam dihedral is also increased for **PhAldDPP N-TBA** (18.7 °) despite both packing in a similar herringbone fashion. The π-π stacking interactions are modulated from a distorted sandwich between lactam and phenyl moieties at short distances (3.76 Å, 3.78 Å) for **PhAldDPP N-EA** to CH- π interactions between lactam and phenyl moieties distorted from ideal orthogonality at elongated distance (4.44 Å) for **PhAldDPP N-TBA**, showing simple chemical modification can have significant impact on the solid-state interactions.

Mobility calculations

Theoretical mobilities based on the crystal structures (Table 3) show at least an order of magnitude improvement in hole mobility of the "planar" **PhEsterDPP NH** (4.70 x 10^{-2} cm^2 $V^{-1}s^{-1}$) compared to the "twisted" **PhEsterDPP N-Hex** (4.00 x 10^{-3} cm^2 $V^{-1}s^{-1}$) and **PhEsterDPP N-TBA** (5.30 x10^{-4} cm^2 $V^{-1}s^{-1}$) systems**. PhAldDPP N-EA** gives rise to theoretical mobility of 3.25x 10^{-2} cm^2 $V^{-1}s^{-1}$, similar in magnitude to **PhEsterDPP NH**, which shares the relatively short lactam-aryl π contacts and hydrogen bonds and reduced dihedral angles. This is an order of magnitude improvement over **PhAcetDPP N-EA** (4.20 x 10^{-3} cm^2 $V^{-1}s^{-1}$), which can be again attributed to the larger twisting of the aryl units out of the plane manifesting in elongated π-πcontacts and the absence of hydrogen bonding.

Electron mobilities generally mirror the trend observed for hole mobilities with **PhEsterDPP NH** (8.2 x 10^{-2} cm^2 $V^{-1}s^{-1}$) showing an order of magnitude improvement vs **PhEsterDPP N-TBA** (6.5 x 10^{-3} cm^2 $V^{-1}s^{-1}$) and two orders of magnitude improvements vs **PhEsterDPP N-Hex** (9.0 x 10^{-4} cm^2 $V^{-1}s^{-1}$). Interestingly, for **PhAldDPP N-EA**, the electron mobility is ten times lower than the hole mobility (3.8 x 10^{-3} cm^2 $V^{-1}s^{-1}$) and this coincides with **PhAcetDPP N-EA** showing a ten times better electron vs hole mobility. (2.9 x 10^{-2} cm^2 $V^{-1}s^{-1}$).

The main charge transport pathways are likely to be along the π stacks, (ESI 1.85-1.89), with sandwich type stacking favoured over the edge to face (CH- π) interactions displayed for the N-alkylated compounds. Molecular packing in a brick wall/lamellar fashion appears to give higher mobility than the classic herringbone, often seen for DPP N-alkyl systems.[23,26] Hydrogen bonding also possesses a contribution by end on overlap. **PhEsterDPP NH** displays a slight reduction in theoretical hole mobility, in comparison to other **PhDPP NH DPPs**.[43] Analysis of previous **PhDPP** based systems shows there is a strong correlation between planarity and theoretical hole mobility,[23,26,43,] with likely the smaller dihedral manifesting in closer face to face π contacts between neighbouring chromophores and shorter hydrogen bonds. In the twisted *N*-alkylated structures (**PhEsterDPP N-Hexyl** and **PhEsterDPP N-TBA**) the likely large planarization that would be undertaken upon doping or excitation relative to the natural ground state, indicated by the higher calculated

reorganisation energies, (ESI 1.85-1.89) would likely result in localised ,self-trapping polarons impeding charge transport,[60] whereas the planarity and extended conjugated backbone of **PhEsterDPP NH** likely affords a larger extended polaron delocalisation length and improved mobility, given the potential for these systems to adopt quinoidal form.

Conclusions

The series of DPPs discussed reported here, display an electron deficient nature evidenced by the multiple reversible reduction processes that are present, bridging the gap in the electrochemical window of electron donor and acceptor DPP systems previously investigated by our group spectroelectrochemically. (Fig. 1). Compounds **PhEsterDPP NH** and **PhAldDPP N-EA** display very similar spectroelectrochemical features, with considerable increases in the molar absorption coefficient for the second reduction process, which we observed previously for pyridinium DPP systems and attributed to adoption of the quinoidal form.[19] On further analysis of the spectroelectrochemical spectra, **PhEsterDPP NH** and **PhAldDPP N-EA** show strong absorption in the near IR region upon reduction, with a shift in λ_{max} from 532 nm (neutral state) to 714 nm (1 electron reduced form) to 833 nm (2 electron reduced form) for **PhEsterDPP NH** and 486 nm (neutral state) to 732 nm (1 electron reduced form) to 867 nm (2 electron reduced form) for **PhAldDPP N-EA**. In comparison, for 4-pyridinium DPP, the λ_{max} of the singly reduced species shows a similar absorption maximum (≈770 nm), however the doubly reduced form is significantly shifted hypsochromically (≈ 640 nm). The increased conjugation of the benzoate and neutrality gives further promise to these compounds use in electrochromic applications in future with strong absorbance approaching the near-IR, and a similar 10-fold increase in absorbance for the doubly reduced form relative to the neutral for **PhEsterDPP NH** and **PhAldDPP N-EA**.[36]

PhAldDPP N-EA, despite *N*-alkylation of the lactam units, displays a relatively planar structure (torsion angles 20.8° and 21.5 °), with similar increases in absorbance in the reduced forms to **PhEsterDPP NH**, with the added advantage of high solubility in a multitude of organic solvents and solvatochromic behaviour. The interplay of intermolecular interactions observed in the crystal structures is seemingly key to this property, given the more twisted **PhEsterDPP *N*-Hex** and **PhEsterDPP *N*-TBA**, do not display the same substantial increase in ε value for the 2-electron reduced form, despite the quinoidal form being predicted computationally, and suffer issues with electrochemical stability.

Theoretical mobility calculations for **PhEsterDPP NH** and **PhAldDPP *N*-EA** show promise for potential use as organic semiconductor systems, giving orders of magnitude improvement in electron and hole transport over the twisted **PhEsterDPP *N*-Hex** and **PhEsterDPP *N*-TBA** compounds, which can be attributed to the relative planarity and close contact interactions, namely π-π stacking and hydrogen bonding. These systems show the importance of how small synthetic modulations to the core DPP chromophore can manifest into large differences in the optoelectronic properties, which is of great interest for future molecular design. Regarding the future outlook for these systems, and soluble **PhDPP**

NHs in general, in addition to the potential electrochromic applications discussed, utilisation as materials for non-aqueous redox flow batteries, charge transfer complexes and sensing and logic gate systems could be realised, given their reversible redox processes and strong absorbance changes.[34,61]

Acknowledgements

We are grateful to the University of Nottingham through the Propulsion Futures Beacon of Excellence, the MICIU/AEI/10.13039/501100011033 for the "Severo Ochoa" program for Centres of Excellence CEX2023-001263-S as well as project TED2021-131911B-I00, and the EPSRC through the LDMI DTP under grant EP/R513283/1. DBA thanks the MICIU/AEI PID2021-123873NB-I00, and the Agència de Gestió d'Ajuts Universitaris i de Recerca (AGAUR), Grant 2021SGR01085. We acknowledge Diamond Light Source for time on I19 under proposals CY21755 and CY28766.

References

1. Chandran D, Lee KS. Diketopyrrolopyrrole: A versatile building block for organic photovoltaic materials. Macromol Res. 2013; 21: 272–283. https://doi.org/10.1007/s13233-013-1141-3

2. Grzybowski M, Gryko DT. Diketopyrrolopyrroles: Synthesis, Reactivity, and Optical Properties. Adv Opt Mater. 2015; 3: 280-320. https://doi.org/10.1002/adom.201400559

3. Tang A, Zhan C, Yao J, Zhou E. Design of diketopyrrolopyrrole (DPP)-Based small molecules for organic-solar-cell applications. Adv Mater. 2017; 29:1600013. https://doi.org/10.1002/adma.201600013

4. Li W, Hendriks KH, Wienk MM, Janssen RAJ. Diketopyrrolopyrrole Polymers for Organic Solar Cells. Acc Chem Res. 2016; 49: 78–85.https://doi.org/10.1021/acs.accounts.5b00334

5. Liu Q, Bottle SE, Sonar P. Developments of diketopyrrolopyrrole-dye-based organic semiconductors for a wide range of applications in electronics. Adv Mater. 2020; 32: 1–46. https://doi.org/10.1002/adma.201903882

6. D. G. Farnum, G. Mehta, G. G. I. Moore and F. P. Siegal. Attempted reformatskii reaction of benzonitrile, 1,4-diketo-3,6-diphenylpyrrolo[3,4-C]pyrrole. A lactam analogue of pentalene. Tetrahedron Lett. 1974; 15: 2549–52. https://doi.org/10.1016/S0040-4039(01)93202-2

7. Li Y, Sonar P, Murphy L, Hong W. High mobility diketopyrrolopyrrole (DPP)-based organic semiconductor materials for organic thin film transistors and photovoltaics. Energy Environ Sci. 2013; 6: 1684–710. https://doi.org/10.1039/c3ee00015j

8. Li W, Wang L, Tang H, Cao D. Diketopyrrolopyrrole-based fluorescent probes for detection and bioimaging: current progresses and perspectives. Dyes Pigments. 2019; 162: 934–50. https://doi.org/10.1016/j.dyepig.2018.11.023

9. Schutting S, Borisov SM, Klimant I. Diketo-pyrrolo-pyrrole dyes as new colorimetric and fluorescent pH indicators for optical carbon dioxide sensors. Anal Chem. 2013; 85: 3271–9. https://doi.org/10.1021/ac303595v

10. Kaur M, Choi DH. Diketopyrrolopyrrole: brilliant red pigment dye-based fluorescent probes and their applications. Chem Soc Rev. 2015; 44: 58–77. https:// doi.org/10.1039/C4CS00248B

11. Ftouni H, Bolze F, Nicoud JF. Water-soluble diketopyrrolopyrrole derivatives for two-photon excited fluorescence microscopy. Dyes Pigments. 2013; 97: 77–83. https://doi.org/10.1016/j.dyepig.2012.11.028

12. Wang J, Hang Y, Hua J. Mannose-functionalized diketopyrrolopyrrole as AIE-active probes for lectin detection and cancer cell imaging. Sensor Actuator B Chem. 2019; 282: 232–42. https://doi.org/10.1016/j.snb.2018.10.091

13. Yang J, Tan H, Li D, Jiang T, Gao Y, Li B, X Qu, J Hua. Synthesis, two-photon absorption and aggregation-induced emission properties of multi-branched triphenylamine derivatives based on diketopyrrolopyrrole for bioimaging. RSC Adv. 2016; 6: 58434–42. https://doi.org/10.1039/c6ra11269b

14. Tang S, Ghazvini Zadeh EH, Kim B, Toomey NT, Bondar MV, Belfield KD. Protein- induced fluorescence enhancement of two-photon excitable water-soluble diketopyrrolopyrroles. Org Biomol Chem. 2017; 15: 6511–9. https://doi.org/10.1039/c7ob01397c

15. Jiang X, Wang L, Tang H, Cao D, Chen W. Diketopyrrolopyrrole: an emerging phototherapy agent in fighting cancer. Dyes Pigments. 2020; 181: 108599. https:// doi.org/10.1016/j.dyepig.2020.108599

16. Cai Y, Si W, Tang Q, Liang P, Zhang C, Chen P, Zhang Q, Huang W, Dong X. Small-molecule diketopyrrolopyrrole based therapeutic nanoparticles for photoacoustic imaging-guided photothermal therapy. Nano Res. 2017; 10: 794–801. https://doi.org/10.1007/s12274-016-1332-2

17. Cai Y, Liang P, Tang Q, Yang X, Si W, Huang W, Zhang Q, Dong X. Diketopyrrolopyrrole–Triphenylamine Organic Nanoparticles as Multifunctional Reagents for Photoacoustic Imaging-Guided Photodynamic/Photothermal Synergistic Tumor Therapy. ACS Nano. 2017; 11: 1054–63. https://doi.org/10.1021/acsnano.6b07927

18. Luňák S, Vala M, Vyňuchal J, Ouzzane I, Horakova P, Moziskova P, Elias Z, Weiter M. Absorption and Fluorescence of Soluble Polar Diketo-Pyrrolo-Pyrroles. Dyes Pigments. 2011; 91: 269-78. https://doi.org/10.1016/j.dyepig.2011.05.004

19. Vala M, Vyňuchal J, Toman P, Weiter M, Luňák S. Novel, soluble diphenyl-diketo-pyrrolopyrroles: Experimental and theoretical study. Dyes Pigments. 2010; 84:176–82. https://doi.org/10.1016/j.dyepig.2009.07.014

20. Vala M, Krajcovic J, Lunak S, Ouzzane I, Bouillon JP, Weiter M. HOMO and LUMO energy levels of N,N'-dinitrophenyl-substituted polar diketopyrrolopyrroles (DPPs). Dyes Pigments. 2014; 106: 136–42. https://doi.org/10.1016/j.dyepig.2014.03.005

21. Vala M, Weiter M, Vyňuchal J, Toman P, Luňák S. Comparative Studies of Diphenyl-Diketo-Pyrrolopyrrole Derivatives for Electroluminescence Applications. J Fluoresc. 2008; 18: 1181–86. https://doi.org/10.1007/s10895-008-0370-x

22. Luňák S, Vyňuchal J, Vala M, Havel L, Hrdina R. The synthesis, absorption and fluorescence of polar diketo-pyrrolo-pyrroles. Dyes Pigments. 2009; 82: 102–108. https://doi.org/10.1016/j.dyepig.2008.12.001

23. Humphreys J, Pop F, Hume PA, Murphy AS, Lewis W, Davies ES, Argent SP, Amabilino DB. Solid state structure and properties of phenyl diketopyrrolopyrrole derivatives. CrystEngComm. 2021; 21: 1796–814. https://doi.org/10.1039/d1ce00039j

24. Murphy AS, Killalea CE, Humphreys J, Hume PA, Cliffe MJ, Murray GJ, Davies ES, Lewis W, Amabilino DB. Ground and excited states of bis-4-methoxybenzyl-substituted diketopyrrolopyrroles: spectroscopic and electrochemical studies. Chempluschem 2019;84:1413–22. https://doi.org/10.1002/cplu.201900286

25. Dhar J, Venkatramaiah N, A A, Photophysical Patil S. Electrochemical and solid state properties of diketopyrrolopyrrole based molecular materials: importance of the donor group. J Mater Chem C 2014; 2: 3457–66. https://doi.org/10.1039/C3TC32251C

26. Dhar J, Karothu DP, Patil S. Herringbone to cofacial solid state packing via H- bonding in diketopyrrolopyrrole (DPP) based molecular crystals: influence on charge transport. Chem Commun. 2014; 51: 97–100. https://doi.org/10.1039/C4CC06063F

27. Pop F, Lewis W, Amabilino DB. Solid state supramolecular structure of diketopyrrolopyrrole chromophores: correlating stacking geometry with visible light absorption. CrystEngComm. 2016;18: 8933-8943. https://doi.org/10.1039/C6CE02157C

28. Data P, Kurowska A, Pluczyk S, Zassowski P, Pander P, Jedrysiak R, Jedrysiak R, Czwartosz M, Otulakowski L, Suwinski J, Lapkowski M, Monkman AP. Exciplex enhancement as a tool to increase OLED device efficiency. J Phys Chem C. 2016;120: 2070–8. https://doi.org/10.1021/acs.jpcc.5b11263

29. Gora M, Pluczyk S, Zassowski P, Krzywiec W, Zagorska M, Mieczkowski J, Lapkowski M, Pron A. EPR and UV–vis spectroelectrochemical studies of diketopyrrolopyrroles disubstituted with alkylated thiophenes. Synth Met. 2016; 216: 75–82. https://doi.org/10.1016/j.synthmet.2015.09.012

30. Debnath S, Park J, Hugar V, Balasubramanyam RKC, Oh J, Kim W, Patil S. Stabilizing Diketopyrrolopyrrole Radical Cations Through Carbazoles: Substitution Pattern vs Spin Delocalization. *J. Phys. Chem. Lett.* 2025; 16: 123–130. https://doi.org/10.1021/acs.jpclett.4c03335

31. Vinutha KV, Rajeswara Rao M. Vinylene-linked diketopyrrolopyrrole chromophores for electrochromism. RSC Adv. 2024; 14:10017–10023. https://doi.org/10.1039/d4ra01280a

32. Rausch R, Röhr MIS, Schmidt D, Krummenacher I, Braunschweig H, Würthner F. Tuning phenoxyl-substituted diketopyrrolopyrroles from quinoidal to biradical ground states through (hetero-)aromatic linkers. Chem. Sci. 2021;12: 793-802. https://doi.org/10.1039/D0SC05475E

33. Quintero SM, Álvaro-Martins MJ, Aranda D, Zheng y, Aragó J, Ortí E, Santos AS, Casado J**.** Neutral and Anion Species of Quinoidal Thienothiophene Diketopyrrolopyrroles Display a Common Aggregation Mode**.** Chem. Eur. J. 2024; 30: e202402094. https://doi.org/10.1002/chem.202402094

34. Sharma S, Rathod S, Yadav SP, Chakraborty A, Shukla AK, Aetukuri N, Patil S. Electrochemical Evaluation of Diketopyrrolopyrrole Derivatives for Nonaqueous Redox Flow Batteries. Chem Eur J. 2021; 27: 12172 – 12180. https://doi.org/10.1002/chem.202101516

35. Humphreys J, Killalea CE, Pop F, Davies ES, Siligardi G, Amabilino DB. Self-assembly of chiral diketopyrrolopyrrole chromophores giving supramolecular chains in monolayers and twisted microtapes. Chirality. 2023; 35: 281-97. https://doi.org/10.1002/chir.23539

36. Humphreys J, Malagreca F, Hume PA, Davies ES, Argent SP, Bradshaw TD, Amabilino DB. Highly electron deficient diketopyrrolopyrroles. Chem Comm, 2023; 59: 1613–16. https://doi.org/10.1039/D2CC06770F

37. Chen Z, Li R, Jia Q, Deng J, Liang D, Cao L, Zhang J, Wang C, Hu J, Shi Y, Zhang H. Dual- Engineered DPP Polymers: Synergistic Hydrogen Bonding and Ring- Fusion for High- Mobility Organic Field- Effect Transistors. Angew. Chem. Int. Ed. 2025; 64: e202514768. https://doi.org/10.1002/anie.202514768

38. Giri D, Saha SK, Anderson I, Chakraborty A, Kala J, Müller JS, Nelson J, Balasubramanyam RKC, Patil S. Delocalized Polarons in Diketopyrrolopyrrole- Based Conjugated Polymers: Implications for Near- Infrared Electrochromism and Beyond. Adv. Funct. Mater. 2025; 35: 2410815. https://doi.org/10.1002/adfm.202410815

39. Wang C, Zang Y, Qin Y, Zhang Q, Sun Y, Di C, Xu W, Zhu D. Thieno[3,2- b]thiophene- Diketopyrrolopyrrole- Based Quinoidal Small Molecules: Synthesis, Characterization, Redox Behavior, and n- Channel Organic Field- Effect Transistors. Chem. Eur. J. 2014; 20: 13755 – 13761. https://doi.org/10.1002/chem.201403037

40. Chen L, Luo N, Hua X, Chen P, Ren P, Zhou Z, Wang Y, Shao X, Zhang H, Liu Z. Synthesis and Optoelectrical Properties of Diene- Containing Diketopyrrolopyrrole- Based Quinoidal Small Molecule. Asian J. Org. Chem. 2025; 14: e202500184. https://doi.org/10.1002/ajoc.202500184

41. Fu L, Fu W, Cheng P, Xie Z, Fan C, Shi M, Ling J, Hou J, Zhan X, Chen H. A diketopyrrolopyrrole molecule end-capped with a furan-2-carboxylate moiety: the planarity of molecular geometry and photovoltaic properties. J Mater Chem A. 2014; 2: 6589–97. https://doi.org/10.1039/C3TA13534A

42. Chen M, Fu W, Shi M, Hu X, Pan J, Ling J, Lia H, Chen H. An ester-functionalized diketopyrrolopyrrole molecule with appropriate energy levels for application in solution-processed organic solar cells. J Mater Chem A. 2013; 1: 105–11.https://doi.org/10.1039/C2TA00148A

43. Głowacki ED, Coskun H, Blood-Forsythe MA, Monkowius U, Leonat L, Grzybowski M, Gryko D, White MS, Aspuru-Guzik A, Sariciftci NS. Hydrogen-bonded diketopyrrolopyrrole (DPP) pigments as organic semiconductors. Org Electron. 2014; 15: 3521–28. https://doi.org/10.1016/j.orgel.2014.09.038

44. Pop F, Humphreys J, Schwarz J, Brown L, Van Den Berg A, Amabilino DB. Towards more sustainable synthesis of diketopyrrolopyrroles**.** New J Chem. 2019; 43: 5783–90.https://doi.org/10.1039/C9NJ01074B

45. Qiao Z, Xu YB, Lina SM, Peng JB, Cao D. Synthesis and characterization of red-emitting diketopyrrolopyrrole-alt-phenylenevinylene polymers. Synth Metals 2010; 160: 1544-1550. https://doi.org/10.1016/j.synthmet.2010.05.019

46. Yang Q, Sun X, Han J, Wang L. Beauty in chemistry: A self-organized and dual-phase emissive diketopyrrolopyrrole derivative as high-yield fluorescent material. Dyes Pigments. 2021;194: 109655. https://doi.org/10.1016/j.dyepig.2021.109655

47. Searle JS, Malagreca F, Denison BMG, Kibler AJ, Walsh DA, Johnson LR, Amabilino DB, Newton GN. Diketopyrrolopyrroles Act as Redox Mediators in Lithium–Sulfur Batteries. ACS Energy Lett. 2025; 10: 2839–2844. https://doi.org/10.1021/acsenergylett.5c01262

48. Erbas SC, Alp S. Synthesis and Spectroscopic Studies of N,N'-dialkyl Derivatives of Antisymmetrical 2H,5H-Dihydropyrrolo[3,4-c]pyrrole-1,4-diones. J Fluoresc. 2014; 24: 329–35 https://doi.org/10.1007/s10895-013-1294-7

49. Szabadai RS, Roth-Barton J, Ghiggino KP, White JM, Wilson DJD. Solvatochromism in diketopyrrolopyrrole derivatives: experimental and computational studies. Aust J Chem 2014;67:1330–7. https://doi.org/10.1071/CH14057

50. Lůnák S, Eliáš Z, Mikyseka T, Vyňuchal J, Ludvíkc J. One electron vs. two electron electrochemical and chemical oxidation of electron-donor substituted diketo-pyrrolo-pyrroles. Electrochim Acta. 2013; 106: 351–59. https://doi.org/10.1016/j.electacta.2013.05.106

51. Moser M, Savva A, Thorley K, Paulsen BD, Hidalgo TC, Ohayon D, Chen H, Giovannitti A, Marks A, Gasparini N, Wadsworth A, Rivnay J, Inal S, McCulloch I. Polarons in DPP Polymers – How Glycol Side Chains and Elongated Conjugated Backbone Influence the Formation and Transport Performance. Angew. Chem. Int. Ed. 2021; 60: 7777 – 7785. https://doi.org/10.1002/anie.202014078

52. Stewart K, Tan E, Kim J, Kim Y, Kim J. Polaron Delocalization in Donor–Acceptor Polymers and its Impact on Organic Electrochemical Transistor Performance. Adv. Electron. Mater. 2026; 0: e00731. https://doi.org/10.1002/aelm.202500731

53. Ray S, Sharma S, Salzner U, Patil S. Synthesis and Characterization of Quinoidal Diketopyrrolopyrrole Derivatives with Exceptionally High Electron Affinities. J Phys Chem C. 2017; 121: 16088–16097. https://doi.org/10.1021/acs.jpcc.7b04085

54. Calvo-Castro J, McHugh CJ, McLean AJ. Torsional angle dependence and switching of inner sphere reorganisation energies for electron and hole transfer processes involving phenyl substituted diketopyrrolopyrroles; a density functional study. Dyes and Pigments. 2015; 113: 609-617. http://dx.doi.org/10.1016/j.dyepig.2014.09.031

55. Fu C, Beldon PJ, Perepichka DF. H-bonding Control of Supramolecular Ordering of Diketopyrrolopyrroles. Chem of Mater. 2017; 29: 2979–87. https://doi.org/10.1021/acs.chemmater.6b05327

56. Mizuguchi J, Grubenmann A, Wooden G, Rihs G. Structures of 3,6-diphenylpyrrolo[3,4-c]pyrrole-1,4-dione and 2,5-dimethyl-3,6-diphenylpyrrolo[3,4-c]pyrrole-1,4-dione. Acta Cryst B. 1992; 48: 696–700. https://doi.org/10.1107/S0108768192003033

57. Mizuguchi J, Takahashi H, Yamakami H. Crystal structure of 3,6-bis(4'-pyridyl)- pyrrolo[3,4-c]pyrrole-1,4-dione, C16H10N4O2, at 93 K. Z Krist NCS 2002; 217: 519–20.

58. Mizuguchi J, Grubenmann A, Rihs G, Structures of 3,6-bis(3-chlorophenyl)pyrrolo[3,4-c]pyrrole-1,4-dione and 3,6-bis(4-chlorophenyl)pyrrolo[3,4-c]pyrrole-1,4-dione. Acta Cryst B, 1993; 49: 1056–60. https://doi.org/10.1107/S0108768193007645

59. Humphreys J, Malagreca F, Hume P, Lewis W, Davies ES, Argent SP, Amabilino DB. Modulation of the optical properties of soluble *N*-alkylated 4-pyridyl diketopyrrolopyrrole derivatives. Dyes Pigments. 2021;109836. https://doi.org/10.1016/j.dyepig.2021.109836

60. Peek MD, Tait CE,Neuhaus P,Fischer GM, Hoffmann M,Haver R, Cnossen A, Harmer JR, Timmel CR, Anderson HL. Electronic Delocalization in the Radical Cations of Porphyrin Oligomer Molecular Wires. Journal of the American Chemical Society. J. Am. Chem. Soc. 2017; 139: 10461–10471. https://doi.org/10.1021/jacs.7b05386

61. Ourgessa MK, McClellan JR, Johnston DH, Mauck CM. Molecular *p*-Doping in Thiophene Diketopyrrolopyrrole Thin Films through Formation of a Charge Transfer Complex. J Phys Chem C. 2023; 127: 18694–18705. https://doi.org/10.1021/acs.jpcc.3c03912